Structure of Reduced Ultrathin TiO x Polar Films on Pt(111)

ARTICLE *in* THE JOURNAL OF PHYSICAL CHEMISTRY C · APRIL 2009

Impact Factor: 4.77 · DOI: 10.1021/jp811020s

THE JOURNAL OF PHYSICAL CHEMISTRY C

Article

Structure of Reduced Ultrathin TiO Polar Films on Pt(111)

Giovanni Barcaro, Stefano Agnoli, Francesco Sedona, Gian Andrea Rizzi, Alessandro Fortunelli, and Gaetano Granozzi

J. Phys. Chem. C, **2009**, 113 (14), 5721-5729• DOI: 10.1021/jp811020s • Publication Date (Web): 13 March 2009

Structure of Reduced Ultrathin TiO_x Polar Films on Pt(111)

Giovanni Barcaro,[†] Stefano Agnoli,[‡] Francesco Sedona,[‡] Gian Andrea Rizzi,[‡] Alessandro Fortunelli,*[,†] and Gaetano Granozzi*[,‡]

Istituto per i Processi Chimico-Fisici (IPCF) del CNR, via Giovanni Moruzzi 1, I-56124 Pisa (Italy), and Dipartimento di Scienze Chimiche and ISTM-CNR, CNR-INFM and INSTM Research Units, Università di Padova

Received: December 14, 2008; Revised Manuscript Received: February 12, 2009

The structure of well-ordered reduced TiO_x nanolayers (NLs) on Pt(111), prepared by reactive evaporation of Ti in an oxygen background and postannealed in different conditions, is discussed on the basis of experimental and theoretical data. All of the observed NLs are formed by a wetting 2D Ti−O bilayer where the Ti atoms are at the interface and the O atoms form the topmost layer. Different structures and stoichiometries depend on the actual Ti coverage and on the conditions of the postannealing. They represent the final products of a self-assembling process where the Ti atoms tend to organize in pseudoepitaxial regions, whereas the O atoms in the topmost layer (more abundant due to stoichiometry constraints) solve the *crowding* problem by creating pseudoepitaxial regions that exhibit dislocation lines and alternate with regions where Ti vacancies (defects or holes) occur. Given the inherent similarity among such reduced phases, as confirmed by an analysis of their electronic structure, it turns out that subtle effects are at the origin of the large variety of possible structures and that kinetic effects during their synthesis can play a role in driving toward a specific phase.

1. Introduction

Nonstoichiometry is a well-known solid-state phenomenon with plenty of examples in the field of transition-metal oxides and sulfides. The availability of different oxidation states of the metal with comparable stability is the factor that limits the phenomenon to a subset of metals: actually, oxides of 3d transition metals of the III−VIII groups are the most representative examples. Because such nonstoichiometric compounds can be stabilized under catalytic conditions (e.g., under reductive conditions), studying their peculiar properties with respect to the corresponding stoichiometric oxides can provide important insights into the innovative properties of an important class of oxide-based functional materials.[1−3] Additionally, in view of the great impact of nanodimensional materials, an important current issue is to understand the relationships between nonstoichiometry and nanodimensionality. Dimensional confinement (nanosystems such as ultrathin films or nanoparticles) may in fact give rise to physical and chemical properties that are quite different from those of the corresponding bulk compounds.[4] When the lowest limit of the ultrathin regime is explored (i.e., when monolayer films are considered, hereafter indicated as nanolayers, NLs), a completely new realm of exotic structures with no counterpart in the bulk may appear[5,6] that has been interpreted as the result of a self-organization of oxide building blocks (i.e., peculiar small MO_x polyhedra) due to specific interactions with the substrate on which the NLs are grown.[7]

Titania is certainly one of the most intriguing materials and one of the best-characterized systems in surface science.[8] Very recently, the relationship between Magnéli-like bulk phases and ultrathin rutile TiO_2(110) films grown on Ni(110) has been evidenced for the first time:[9] the authors interpreted the structure of the ultrathin films as a result of the action of crystallographic shear planes, and the reduction behavior of the ultrathin titania was related to that of the rutile TiO_2(110) surface.

During the past few years, some of us have been involved in the preparation and characterization of ultrathin TiO_x films (the TiO_x notation in place of TiO_2 indicates that some of the films are substoichiometric, i.e., $x < 2$) on Pt single crystals.[10−13] Such studies were originally stimulated by the promotion properties of Pt in photocatalysis[2] and by the fact that Pt/TiO_x is the prototypical system showing the strong metal support interaction (SMSI) effect.[14] Such an interest has grown during the various stages of the project due to the wide range of structures found on Pt(111). In fact, it was shown that, by varying the growth parameters, deposition of understoichiometric TiO_x NLs can yield several different phases, each having a distinct low energy electron diffraction (LEED) pattern.[10] The combined use of LEED and high-resolution scanning tunneling microscopy (STM) showed that each of them corresponds to large domains with either hexagonal or rectangular unit cells. The hexagonal structures can either be arranged in a so-called wagon-wheel-like lattice[11] or in a kagomè-like lattice.[10] Some of the rectangular structures are characterized by a peculiar zigzag-like appearance.[12,13] Moreover, both hexagonal and rectangular structures can either be commensurate or incommensurate.

In previous articles, we have reported the experimental results on preparation[10]and characterization (both spectroscopic[15] and structural[10,11]) of the whole series of reduced TiO_x/Pt(111) NLs. However, whereas the geometric structure of two of such reduced NLs has been already reported,[12,13] a description of their electronic structures and stoichiometry evolution in the light of a unifying theoretical framework is still lacking. In this article, we report a comprehensive investigation where both structural and electronic properties of reduced TiO_x/Pt(111) NLs are discussed on the basis of density functional (DF) calculations. In particular, we will focus attention on the comparison with the STM images and on the interpretation of the black features, which have been interpreted as pico-holes, that is defective sites

* To whom correspondence should be addressed. E-mail: fortunelli@ipcf.cnr.it(A.F.), gaetano.granozzi@unipd.it (G.G.).
[†] Istituto per i Processi Chimico-Fisici (IPCF) del CNR.
[‡] Università di Padova.

10.1021/jp811020s CCC: $40.75
Published on Web 03/13/2009

with Ti vacancies that expose the bare Pt(111) support. These defects have been shown to be common in oxide-on-metal substoichiometric ultrathin films,[13,16] and to ensure them peculiar properties, such as the possibility of acting as trapping and nucleation centers of adsorbed species, thus making these systems able to function as nanotemplates.[17−20] The DF data will be also employed to discuss valence band photoemission spectroscopy (VB-UPS) experimental data.[15] VB-UPS has long been established as a valuable technique to investigate the reactivity of surfaces as it allows one to identify the electronic states involved in the surface chemical processes. A thorough characterization of the electronic structure of such novel interfacial phases, that are potentially relevant for chemical applications, might help to understand their properties. In addition, studying TiO_x films in the single-layer regime may allow one to identify the role of extreme 2D confinement, the role played by defects, and the mixing between the NL and metal substrate electronic states.

2. Computational and Experimental Methods

DF calculations have been performed using the PWscf (Plane-Wave self-consistent field) computational code,[21] employing ultrasoft pseudopotentials.[22] A total of 6, 12, and 10 electrons are explicitly considered for O, Ti, and Pt, respectively. The PW91 exchange-correlation functional,[23] which is a gradient-corrected functional, has been used. On the basis of previous experience on this system,[12,13,20] values of 30 Ry on the energy cutoff for the selection of the plane wave basis set for describing the wave function and of 150 Ry for describing the electronic density, respectively, have been demonstrated to provide accurate results (1 Ry = 13.606 eV). All of the calculations have been performed applying a smearing procedure of the energy levels with a Gaussian broadening of 0.002 Ry. Because of the intrinsic polarity of the oxide layer, the unit cells have been built in such a way to leave about 8−10 Å of empty space between replicated cell in the direction perpendicular to the surface. A dipole correction[24] has been applied to correct for the artificial electric field across the slab. The dimension of the unit cell, the numbers of Pt layers used to describe the underneath metal support, and the sampling of the Brillouin zone are parameters that have been tuned on the basis of the particular phase considered, and further details will be given in the following. For all of the TiO_x phases considered, local relaxations of the oxide structure have been performed by freezing the positions of the Pt atoms of the metal support until the forces on the atoms were smaller than 0.01 eV/Å. Simulated STM images are obtained using the Tersoff−Hamann approach.[25] Note that we chose a gradient-corrected exchange-correlation functional appropriate for these ultrathin substoichiometric *polar* oxide phases, as we believe that the strong influence of the underlying metal support and the conductive character resulting from the metallization of the oxide monolayer as the main depolarization mechanism (the discussion below) advise against the use of DFT+U methods or hybrid[26] exchange-correlation functionals that have recently been proposed for defected or doped (and thus in some sense reduced) stoichiometric titania phases.[26,27] In other words, we do not think that electron localization due to correlation effects (i.e., the phenomenon that the U term in the DFT+U method or the Hartree−Fock exchange component in the hybrid methods are called to describe) is effective for these systems. This seems to be confirmed by the reasonable agreement between predicted and experimental VB-UPS spectra that will be discussed in section 3.2. Further studies would anyway be required to further clarify this point and are planned in future work.

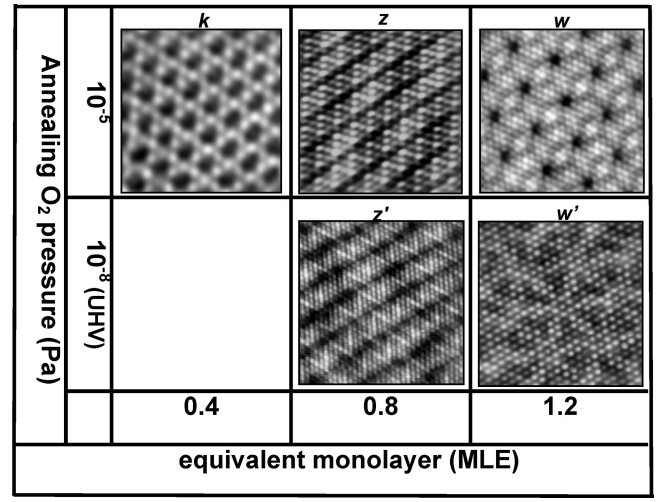

Figure 1. Summary of the STM constant-current images of the TiO_x/Pt(111) NLs so far characterized:[10] the different phases are categorized according to the oxygen pressure of the annealing procedure and to the nominal coverage in MLE (text). k = kagomé, z = zigzag-like, w = wagon-wheel-like.

The preparation and structural characterization of the herein discussed NLs have been reported in detail elsewhere.[10] The prepared ultrathin films were completely wetting the substrate surface as checked by using CO as chemisorption probe. The photoemission experiments were carried out on the Material Science beamline at Elettra in Trieste, Italy.[28] This beamline takes light from a bending magnet source and mounts a plane grating monochromator. The experimental end station is provided with a Phoibos 150 mm (SPECS GmbH) multichanneltron analyzer. The XPS data were collected at 650 eV photon energy, whereas VB-UPS data were collected with a 200 eV photon energy and with an overall energy resolution of 0.5 and 0.15 eV, respectively. All of the photoemission data were acquired at normal emission.

The STM are taken at room temperature (RT) in an Omicron VT-STM system operating at a base pressure of 5×10^{-9} Pa. The system is equipped with four-grid LEED optics. Pt−Ir tips were used in all of the experiments. Tunneling voltages are given with respect to the sample. The tunneling parameters are reported in the corresponding captions of the reported STM images. The scanner was calibrated in the z direction with respect to the step edge of the clean Pt(111) surface. For the lateral calibration, a (2×1) reconstructed Pt(110) surface has been used.

3. Results and Discussion

In Figure 1, we report a summary of the different reduced TiO_x NLs so far characterized: the reported STM images furnish a rationale for the labels used to identify each one of them (k stands for kagomè, i.e., in Japanese bamboo basket,[29] z and z' stand for zigzag, w and w' stand for wagon-wheel). Our current DF-based study will be confined to the k, z, z', and w NLs, which represent the observed systems when the nominal coverage (expressed in monolayer equivalent, MLE, ref 10 for details of its definition) is increased from 0.4 to 1.2 MLE. It should be stressed that the actual coverage is related to the NL density rather than to the fraction of the Pt(111) surface uncovered, as evidenced by previous STM investigation, which demonstrated a full wetting of the substrate.[10] When the z-NL is subjected to UHV annealing, a new zigzag-like phase, namely z', with a significantly larger unit cell is obtained.

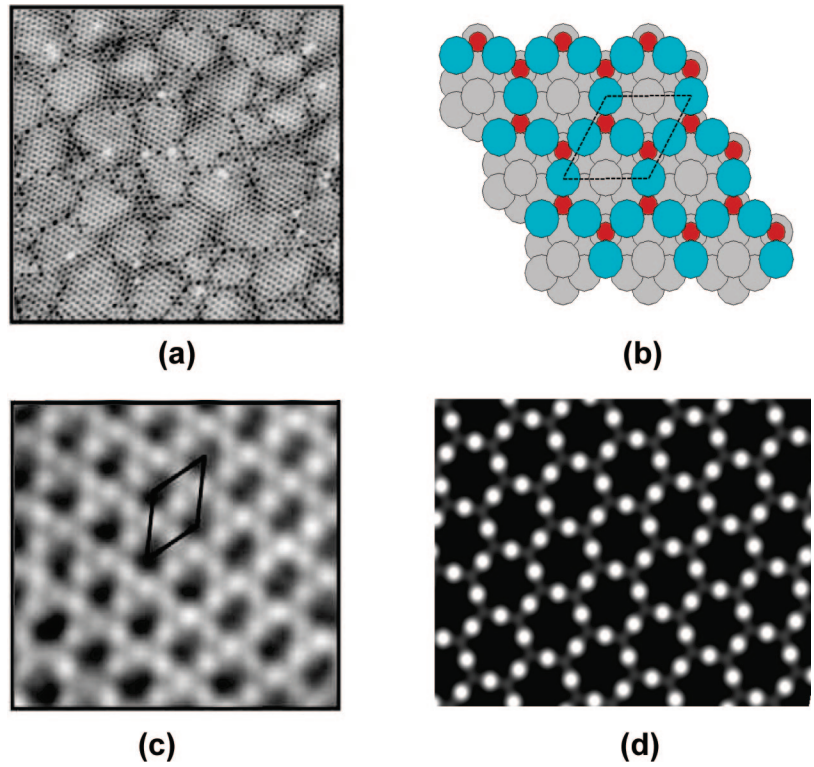

Figure 2. *k*-TiO_x/Pt(111) NL: (a) large-scale STM constant-current image (300 × 300 Å^2, $V = 1$ V, $I = 1.0$ nA); (b) proposed structural model (Pt atoms are depicted in gray, Ti in red, and O in light blue); (c) high-resolution (30 × 30 Å^2, $V = -0.4$ V, $I = 1.06$ nA) STM constant-current image; (d) theoretically simulated STM image at, $V = -0.4$ V.

In the following, we first describe (section 3.1) the DF-derived structural models and compare with STM data of each of the NLs, that is, *k*, *z*, *z*′, and *w*, with particular emphasis on those herein reported for the first time (*k* and *w*). Note that structural assignements based on the coincidence of experimental and theoretically simulated STM images are not definitive, as the solution is not univocal. Therefore, to support these assignements, subsequently in section 3.2 we also address the electronic structure problem and compare the DF-derived data with photoemission data.

3.1. Structural Models and STM Data. ***3.1.1. Kagomè-like Nanolayer.*** At low Ti coverage (0.4 MLE) and after annealing the sample at a temperature of 673 K in an oxygen pressure of about 10^{-5} Pa (Figure 1), the *k*-NL is obtained. The LEED pattern indicates an incommensurate and hexagonal superstructure of the oxide. The evaluation of diffraction spots yields a (2.15 ± 0.05) × (2.15 ± 0.05) superstructure with respect to the Pt(111) substrate, which corresponds to an overlayer lattice constant equal to 6.0 ± 0.1 Å, aligned along the $\langle 1\bar{1}0 \rangle$ direction of Pt(111).[10] Part a of Figure 2 reports a large-scale empty-states STM image of the *k*-NL (taken at a positive bias). It is clearly evident that this phase forms a patched 2D overlayer and that the dark spots form a hexagonal lattice with a unit cell of dimensions very close to those obtained by LEED. In some images, a rather ordered modulation of the hexagonal mesh with a periodicity of about 35 Å is visible, likely to be associated with a Moiré-like pattern. Actually, by superimposing the overlayer and substrate unit cells it is easy to verify that 6 unit cells of the *k*-NL are commensurate with 13 cells of the Pt(111) substrate. In analogy with the other reduced phases, the *k*-NL is composed of a Ti−O bilayer in which Ti is located at the interface with the substrate. The resulting structure exhibits a hexagonal surface mesh with a periodicity of approximately 6.0 Å, in good agreement with the hexagonal 2.15 × 2.15 mesh seen by LEED. This value, divided by two, is in the range of O−O distances in bulk titanium oxides, which vary between 2.53 Å (brookite) and 3.07 Å (Ti_2O_3).

As the Pt(111) and the *k*-NL are incommensurate, to model the latter at the DF level we chose to employ a hexagonal unit cell of 6.0 Å side length, corresponding to the lattice parameter of the oxide, superimposed to a strained (2 × 2) Pt(111) surface with a lattice parameter elongated from 2.775 to 3.00 Å. As alternative solutions, a hexagonal unit cell of 5.55 Å (2.775 Å × 2) side length was also considered, in which the oxide, instead of the metal slab, was compressed, and a compromise unit cell in which the oxide was slightly compressed and the metal substrate slightly expanded. In analogy with previous work on the *z*-NL,[12] we performed test calculations by adopting all of these three solutions, obtaining qualitatively similar results, and in the following only the results obtained using an unstrained oxide will be reported. Because of the reduced dimensions of the unit cell, for this phase it was computationally feasible to use up to 8 Pt layers to describe the metal support, and we were able to check that the structural and energetic asymptotic behavior is essentially reached using 4 metal layers. A fine (6,6,1) k-point grid for the description of the first Brillouin zone was employed.

On the basis of the STM image shown in Figure 1 and under the hypothesis that at negative bias the negatively charged oxygen ions are imaged (current tunneling from valence occupied states), the model structure shown in part b of Figure 2 can be devised. The unit cell (shown in dashed lines) contains two Ti atoms forming a honeycomb lattice and three O atoms forming a kagomé pattern; the stacking is such that O atoms are in the topmost layer. The stoichiometry of the phase is thus Ti_2O_3 ($x = 1.5$), with a Ti^{3+} formal oxidation state, so that this

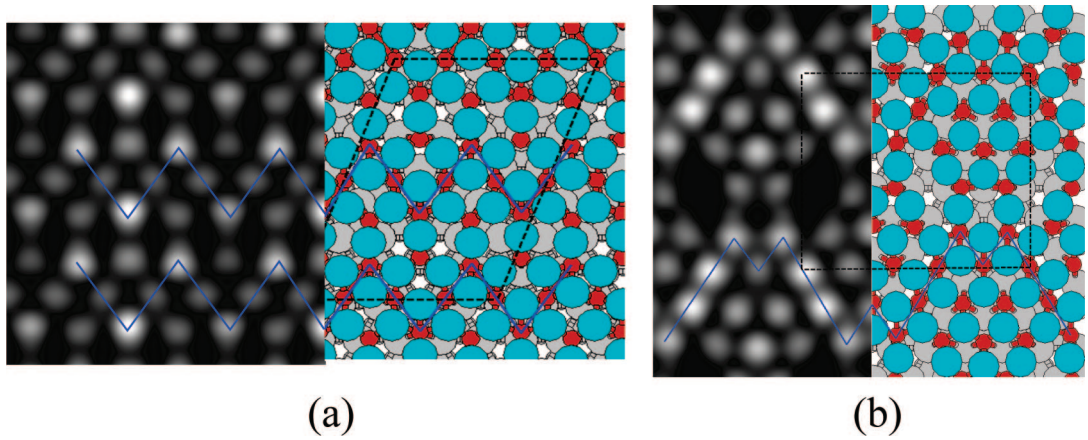

Figure 3. STM constant-current simulated images and structures of (a) the z-TiO_x/Pt(111) and (b) the z'-TiO_x/Pt(111) NLs. Both STM simulations are done at +1.0 V at 2 Å above the height of the O layer. The blue lines highlight the zigzag-like motif which has the shape of a V (z) or W (z'). The dashed black lines encircle the unit cells employed in the DF calculations. Color coding as in Figure 2.

phase results in the most oxidized among those considered in the present work.

According to the stoichiometry of the oxide, the ratio among the number of Ti atoms and of surface Pt atoms is around 0.5, in agreement with the experimental determination of the Ti coverage. In parts c and d of of Figure 2, we present a comparison of the experimental − part c − and simulated − part d − STM images of the k-NL, both at −0.4 V bias. Confirming our assumption, the O atoms are visible in the STM images, with a full agreement between theory and experiment. The Ti atoms are oxidized and, at negative bias, the current tunnels from the full *sp* states of the oxygen ions.

A further confirmation of the correctness of the structural model of part b of Figure 2 comes from the agreement between experimental and theoretical mobility data of Au atoms on the k-NL,[30] where it was found that Au deposition on the k- NL gives rise to extremely small clusters (around 0.2 nm in size) and that this finding can be rationalized by considering that each hexagonal unit presents a pico-hole acting as a strong trapping center for Au atoms, which (once trapped) can detach from it only overcoming an energy barrier of 2.4 eV. These pico-holes (whose density is very high, one pico-hole every 6 Å^2) are surrounded by two hexagons, one of Ti cations at a lower height and one of O anions in the topmost layer, rotated by 30°. The hexagons share common edges where each Ti ion is coordinated by three O ions and each O ion is coordinated by only two Ti ions.

3.1.2. Zigzag-like Nanolayers. By increasing the Ti coverage, we obtain two zigzag-like NLs, called z and z' (Figure 1). The z-NL is obtained at the same oxygen pressure of the k one, but at a higher Ti coverage, whereas the z'-NL is obtained at a nominal pressure of 10^{-8} Pa. With respect to the k, these NLs are thus more reduced. Their structures have been deeply analyzed elsewhere[12,13] and we only briefly summarize here the major points. In Figure 3, the structures of z (a) and of z' (b) are shown, with the respective simulated STM images at positive bias. A comparison between Figure 1 and 3 highlights the agreement between theory and experiment.

The z-NL is characterized by a rectangular incommensurate unit cell of 6.8 Å × 8.6 Å; its stoichiometry is Ti_6O_8 ($x = 1.33$), corresponding to a formal oxidation state of $Ti^{+2.67}$. To model this phase, the unit cell employed has been the one depicted in part a of Figure 3, which corresponds to a stretching of the Pt lattice parameter of about 2% along two perpendicular directions. On the contrary, the z'-NL is commensurate with the substrate and is characterized by a rectangular unit cell of 16.6 Å × 14.4 Å; the stoichiometry is $Ti_{24}O_{30}$ ($x = 1.25$), corresponding to a formal oxidation state of $Ti^{+2.5}$. For both phases, the stacking of the ions is such that the oxygens form the topmost layer (as in the case of k). The ratio among number of Ti atoms and number of Pt atoms at the surface results in 0.67 in both cases, in reasonable agreement with the experimental data of a nominal coverage of 0.8 ML.

Let us now discuss the STM data. First of all, in this case we consider positive bias, so that the current tunnels through empty states above the Fermi level. We thus expect that tunneling will occur in particular through the empty *d* states of the oxidized Ti atoms. Second, the STM images of both phases are characterized by two types of Ti atoms, some brighter than some others; in particular, the V and W shape of the zigzag-like motifs of the two NLs is determined by a running sequence of brighter spots. This effect is essentially electronic in nature: by considering the structure of the two phases, we can see that the brighter spots correspond to four-coordinated Ti ions (Ti_4), whereas the darker ones to three-coordinated Ti ions (Ti_3). The Ti_4 are thus more electron-depleted than the Ti_3 (having a greater number of O atoms around them) and consequently have a higher density of empty states and appear thus brighter in the STM images. Note that, to simulate the z-NL without exceeding our computational resources, we had to impose a commensurate relationship between the oxide and metal slabs and thus a topographic relationship of the Ti atoms relative to the underlying Pt(111) lattice, in contrast to experimental (and also theoretical) evidence that the oxide/support interaction is essentially nondirectional;[12] this makes the agreement between simulated and experimental STM pattern worse in this case.

Finally, we can note that these zigzag-like NLs are both characterized by triangular regions with a close-packed arrangement of Ti and O atoms, separated by dislocation lines which are necessary to solve the *crowding* problem due to a lattice mismatch between the Pt(111) and the oxide film and intercalated by less dense regions constituted of bridging oxygens (z) or defective Ti_2O_3 units (z'). The main difference between the two NLs is that the less dense regions in z do not present pico-holes, but only a lack of Ti atoms that however does not lead to defective sites, whereas in z' these regions are constituted by defective units in which real holes are present (having an elliptical shape).[13] Actually, in the z'-NL a variable degree of

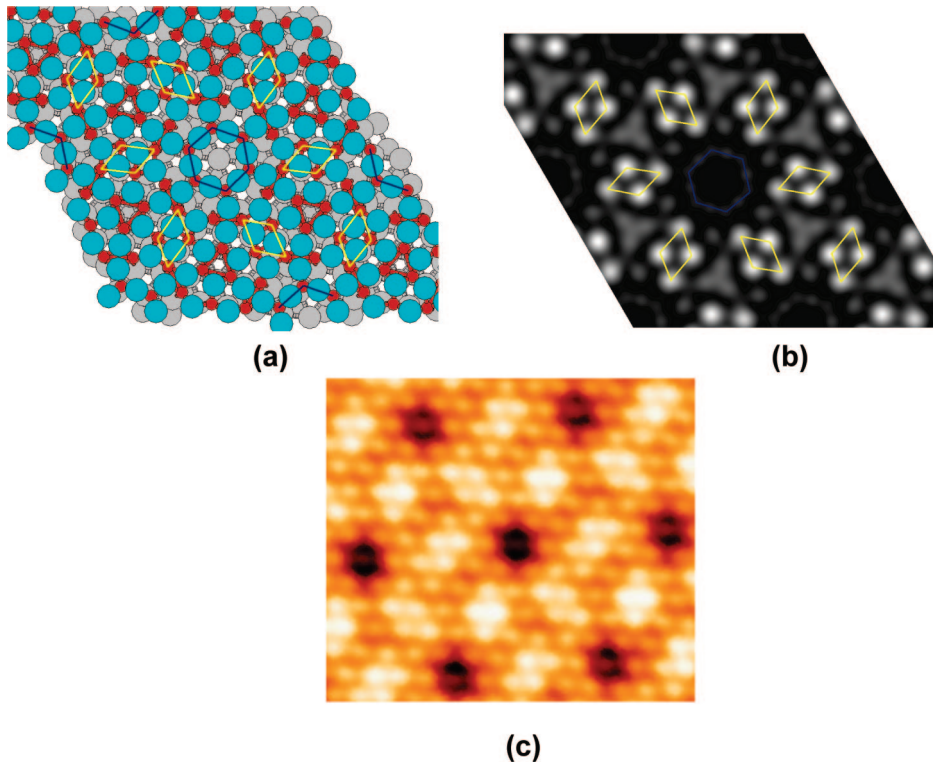

Figure 4. *w*-TiO_x/Pt(111) NL: (a) DF-derived structural model: yellow segments link the Ti_4 atoms; blue segments link the six Ti_3 atoms at the border of the central cavity; (b) simulated constant-current STM image at +1.0 V; (c) experimental constant-current STM image at +1.0 V. In (a), color coding as in Figure 2.

defectivity is observed depending on the actual post annealing time; in fact, in the experimental conditions typically employed for the synthesis of *z*′, there is a strong competition among phases with different morphologies, defectivities, and stoichiometries (discussion in ref 13). For example, at the same stoichiometry of the structure shown in part b of Figure 3 and only 1 eV above in energy, an alternative structure deriving from the rearrangement of the O atoms in the trough determines the formation of another type of pico-hole (a round defect similar to that of the *k*-phase, see the dotted white circles in part a of Figure 1 and in part b of Figure 4 of ref 13). The presence of these different types of pico-holes is the reason why *z*′ acts as a nanotemplate, as already proven by STM measurements on Au deposits on the *z*′-NL.[19]

3.1.3. Wagon-Wheel-like Nanolayer. At the same oxygen pressure of the *k*- and *z*-NLs, but increased Ti coverage, another phase, named *w* from wagon-wheel, is obtained. Such wagon-wheel-like topology is quite common in ultrathin oxide films and in a previous article we have discussed thoroughly its peculiarities and compared with the experimental data of the *w*-NL with the literature data of several different NLs.[11]

The *w*-NL is characterized by a $(\sqrt{43} \times \sqrt{43})R7.6°$ commensurate hexagonal unit cell of 18.2 Å and the corresponding STM pattern has been qualitatively discussed on the basis of a Moiré-like model, that is as deriving from a modulation of the Ti occupancy of the different substrate sites (i.e., hollow, bridge, and on-top sites).[11] However, this Moiré-like model did not furnish any hypothesis on the nature of the hexagonally arranged black features detected by STM (part c of Figure 4). The model we propose here leads to a very good agreement with the experimental STM images (below) and is also entirely consistent with those proposed for the other TiO_x NLs. It has a $Ti_{30}O_{36}$ ($x = 1.2$) stoichiometry (i.e., $Ti^{+2.4}$ formal oxidation state) and the same stacking of the already discussed NLs, that is, characterized by an oxygen topmost layer.

Given the large dimensions of the unit cell, the metal support has been modeled by using only two Pt layers and the description of the first Brillouin zone has been performed at the Γ point (calculations with a greater number of k-points do not introduce any qualitative change in the results). By inspecting the STM image at positive bias (shown in part c of Figure 4), we can note that, as in the case of the zigzag motifs, also in this case we can distinguish between brighter and less bright Ti atoms. On the basis of previously derived building principles,[13] we have thus developed the model shown in part a of Figure 4. This structure can be roughly described as composed of a close-packed arrangement of Ti atoms with an oxygen layer on top, such that the brighter Ti atoms in the experimental STM image are four-coordinated (Ti_4), whereas all of the other Ti atoms (which appear darker in the STM image) are three-coordinated (Ti_3). Note that we have managed to achieve this result by keeping the full 6-fold symmetry characterizing the structure. The circular black features appearing in the STM images are, in our model, real holes in which the underlying metal support is exposed. These pico-holes are analogous to those found in the *k*-phase − part b of Figure 2 − with the difference that in the *w*-phase their density is much lower (one hole per 18.2 $Å^2$ instead of one hole per 6 $Å^2$) and they are surrounded by compact regions with a close-packed arrangement of Ti and O ions, whereas in the *k*-phase they are surrounded by similar defective sites. In analogy with the *k*-phase, we could think that also in the *w*-phase the pico-holes can play the role of trapping and nucleation centers, for example, toward the adsorption of metallic atoms, clusters, or toward organic molecules. However, it should be kept in mind that, the oxidation state of the Ti ions in the two NLs being different as

well as the environment of the pico-holes, the long-range electrostatic field can determine a different chemical and adsorption behavior. Indeed, attempts to demonstrate that the pico-holes of the *w*-phase act as trapping centers for the growth of deposited Au atoms have so far failed.

By looking at the simulated STM image (part b of Figure 4), we can see that our model is successful in explaining the observed STM contrast. The present DF analysis discards the previous interpretation, which correlated the brightness in the STM images with the positions of the Ti atoms with respect to the Pt atoms in the metal support: in particular, it was previously proposed that atoms sitting in bridge sites with respect to two underneath Pt atoms appeared brighter than atoms sitting in hollow or top positions.[11] On the contrary, the contrast is essentially electronic in nature, as in the previously examined *z* and *z*' cases. In fact, the Ti_4 atoms, connected by yellow segments in part b of Figure 4, are brighter, whereas the Ti_3 atoms are darker. However, within the subset of Ti_3 atoms, the ones at the border of the pico-holes are the darkest. This is due to a general behavior of Ti atoms by which the correlation between Ti-coordination and brightness of the STM spots can be lost outside compact close-packed regions. If we look at the six Ti atoms forming the central hexagon (blue line connecting Ti atoms in Figure 4), we can note that they alternate with another hexagon of O atoms: as these O atoms are only 2-fold coordinated, to compensate their low coordination they interact via partially covalent bonds with the metallic substrate underneath. The final result is that they receive electronic charge from the Pt slab and are thus not capable of oxidizing the neighboring Ti atoms. These Ti atoms, as a consequence, appear darker in the STM images because of a reduced density of empty states above the Fermi level. We call this behavior general because the same effect was observed for the Ti atoms at the border of uncoupled stripes in models of the *z*′-phase in parts d and e of Figure 2 in ref 13. Most probably this is also the reason why in the case of the *k*-NL it has not been possible to obtain high-resolution images at positive bias: in the *k*-NL, in fact, as already discussed, all of the O ions are doubly coordinated by counterions and, consequently, all of the Ti ions of the structure result weakly oxidized.

Despite the essentially good agreement between experimental and simulated STM images, which makes us confident that a qualitative understanding of its basic structure has been achieved, there are still open questions concerning this NL. The main issue is that in this case the predicted Ti coverage (0.7 MLE) does not match the experimentally derived one (1.2 MLE). We have explored in depth various possibilities to increase the Ti coverage but found essentially that − to reach a coverage of (at least) 1 MLE − a TiO_x bilayer must necessarily be invoked. This, however, is in contradiction with experimental evidence based on photoelectron diffraction data,[11] which shows that the O 1s intensity is not modulated and thus that oxygens form an uppermost monolayer. One is therefore forced to hypothesize that some of the deposited Ti atoms do not stay in the TiO_x film, but intermix with the support, finally producing some sort of Pt/Ti surface alloy,[31] as already hypothesized in the literature for the TiO_x/Pd(111) system.[32] An indirect support to this hypothesis comes from the fact that the structure depicted in part b of Figure 4 is indeed a stable local minimum but that other more stable structures with the same stoichiometry can also exist, for example one exhibiting a pin-wheel habitus similar to that found for the TiO_x/Pd(111) system.[32] A pinning of the proposed *w*-phase by Ti atoms intermixed with the Pt support, or kinetic trapping effects, could explain this puzzle. Note that kinetic effects were also found to appreciably influence the morphology of the *z*′-NL.[13] It is thus to be stressed that the phenomenology of these TiO_x/Pt(111) NLs does not seem to be fully ruled by thermodynamics, which is different from other systems.[33] In this connection, it can be noted that very recently it has been demonstrated that TiO_x NLs can be directly obtained by the controlled oxidation of Ti/Pt surface alloy.[34]

TABLE 1: DF-Derived Energetics of the Herein Investigated TiO_x NLs[a]

TiO_x NL	stoich. (*x*)	E_T (eV)	E_{adh} (eV)	E_{ox} (eV)
k	1.5	−18.533	2.911	−15.622
z	1.33	−17.323	2.717	−14.606
z′	1.25	−16.843	2.996	−13.847
w	1.2	−16.197	2.823	−13.374

[a] E_T is the total energy of the oxide system, that is the energy difference between the total energy of the composite oxide-on-metal system minus the energy of the free-standing Pt(111) slab and the isolated Ti and O atoms; E_{adh} is the adhesion energy in absolute value, that is the energy lost in separating the oxide and the Pt(111) slabs with their atomic structure kept frozen; E_{ox} is the *pure* oxide energy, that is E_T minus the adhesion energy (taken with its sign). All of the quantitities are given per Ti atom and in electron volts.

3.1.4. Energetics of the TiO_x NLs. We conclude this section with a brief analysis of the energetics of the four TiO_x NLs. In Table 1, we report the following quantities: (a) the total energy of the oxide system (E_T), that is the energy difference between the total energy of the composite oxide-on-metal system minus the energy of the free-standing Pt(111) slab and the isolated Ti and O atoms; (b) the adhesion energy (E_{adh}) in absolute value, that is the energy lost in separating the oxide and the Pt(111) slabs with their atomic structure kept frozen; and (c) the *pure* oxide energy (E_{ox}), that is E_T minus the adhesion energy (taken with its sign). All of the quantitities are given per Ti atom and in electron volts.

The numbers reported in Table 1 lend themselves to two interesting considerations. First of all, the adhesion energies of the *k*- and *z*′-NLs are similar, whereas those of the *z*- and *w*-NLs are appreciably smaller. In the case of the *w*-NL, this is justified by the fact that the compact regions of this phase are arranged in an hexagonal pattern that does not have a good epitaxy to the underlying Pt(111) support, whereas in the case of the *z*-NL this is due to the presence of large troughs composed of bridging oxygens that do not contribute much to the adhesion energy. Apart from these subtle variations, however, it can be noted that the total energies of the oxide system are in very good approximation directly proportional to the formal charge state (the stoichiometry) of the Ti atom. This confirms a basic analogy among these reduced phases, whose constitution can be rationalized in terms of a common set of building principles.[13]

3.2. Electronic Structure and Photoemission Data. The core level and VB-UPS data of the *z*, *z*′, and *w* NLs have been already reported and discussed qualitatively.[15] The photoemission data relevant for the forthcoming discussion are summarized in Figure 5. The Ti 2p binding energy (BE) is typical of reduced Ti (456.4 eV), but we deem that BE value is mainly dictated by the location of the Ti atoms at the interface with the Pt support: the data so far obtained[10,15] clearly indicate that the typical BE values of the actual stoichiometric titania (458−459 eV) is only seen when the Ti atoms are sandwiched between two oxygen layers. No appreciable Ti 2p BE shift (Figure 5) could be seen along the series of reduced NLs despite of the actual formal oxidation state of the Ti atoms derived from the models discussed in the previous sections. The O 1s spectra

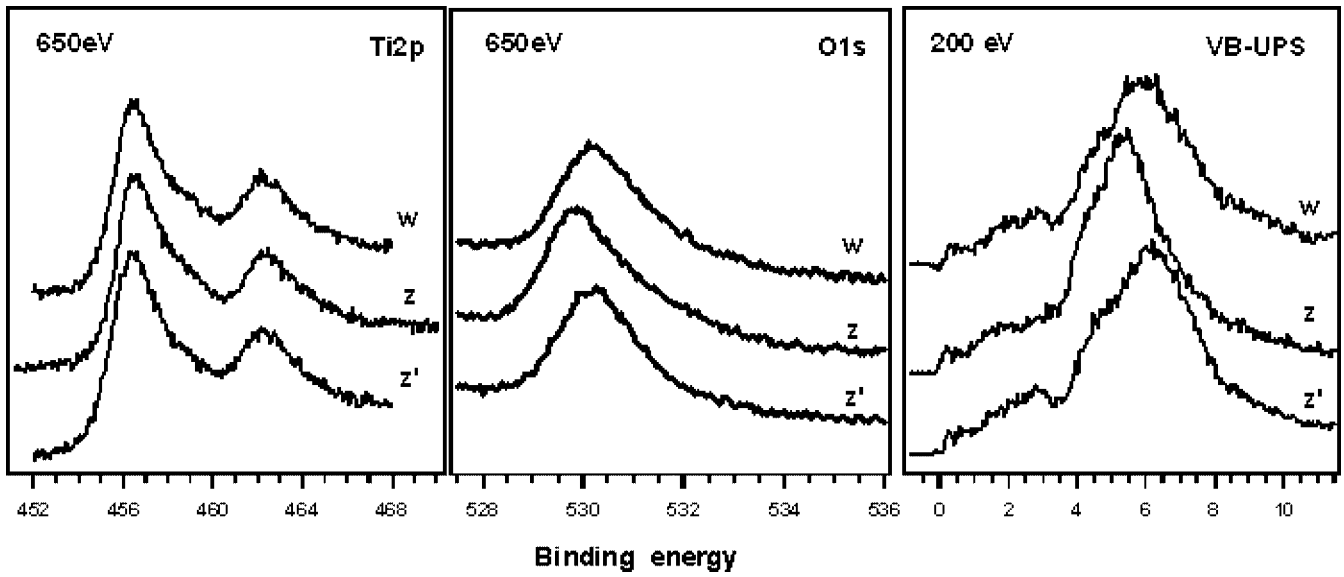

Figure 5. Core level (Ti 2p and O 1s) and VB-UPS data of *w*-, *z*-, and *z*′-TiO_x/Pt(111) NLs (ref 15). The reported VB-UPS data were obtained after subtraction of a normalized clean Pt(111) spectrum (ref 15 for details on the subtraction procedure).

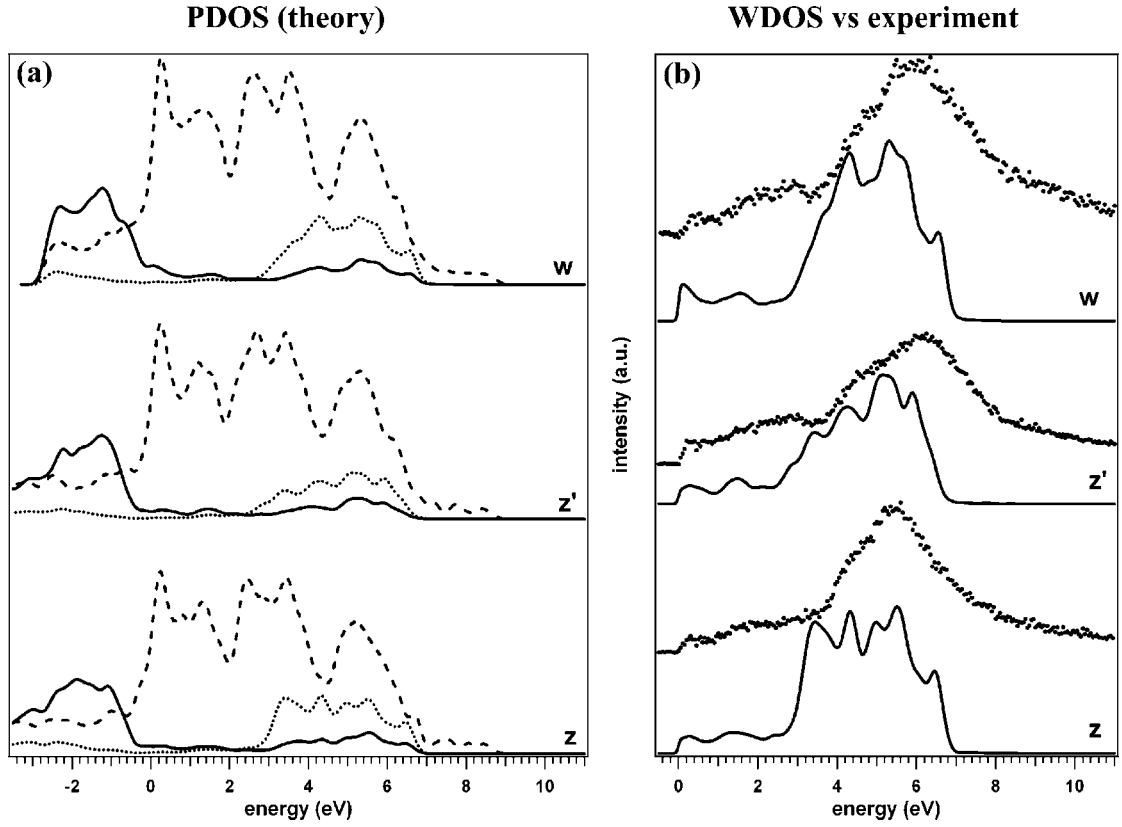

Figure 6. (a) Theoretical PDOS (---Pt, ····O, — Ti contributions) of *w*-, *z*-, and *z*′-TiO_x/Pt(111) NLs and (b) comparison between the WDOS and the experiment (ref 15). See the text for the definitions.

(Figure 5) are similar in all of the reduced phases, but one can observe a slight shift in the position of the peak to higher BE on passing from *z*- to the other two reduced NLs. This phenomenon can be better discussed after an analysis of the VB-UPS data.

The VB-UPS data, obtained with a photon energy of 200 eV to minimize the contribution from the Pt substrate states and after a subtraction of the contribution from the clean substrate (as described in ref 15) is reported in Figure 5; in the original interpretation of the experimental data,[15] the occurrences of the low intensity features in the low BE region (close to the Fermi edge) were interpreted as arising from a strong intermixing between the Pt substrate and the NL states. This point and the shift in the position of the VB-UPS main peak centered around 6−7 eV to higher BE in passing from the *z*- to the *z*′- and *w*-NLs (analogous to the shift in the O 1s BE in the XPS data, see above) can be discussed on the basis of the present DF data.

In part a of Figure 6, we show the projected density of states (PDOS) for the *z*-, *z*′-, and *w*-NLs as decomposed into their Ti, O, and Pt contributions. To properly compare them with the VB-UPS data, in part b of Figure 6 we report also the weighted density of states (WDOS), which takes into account the experimental cross-section at the used photon energy. The WDOS curves were computed by applying a Gaussian broadening of 0.2 eV to the monoelectronic levels, after weighting them by the photoionization cross sections and using tabulated values for the atomic subshell cross sections.[35]

Because we compare the WDOS with the experimental VB-UPS data where the clean Pt(111) substrate contribution has been substracted, only the O and Ti PDOS factors have been considered. It can be underlined that the low-intensity experimental features observed in the low-BE region, previously assigned to the NL-Pt hybridization, are correctly predicted by the theory even neglecting the Pt contribution to the WDOS. This suggests that they are rather to be assigned to Ti 3d states peculiar to these reduced phases than to Pt states: the presence of states close to the Fermi energy is a further confirmation of the metallic character of these interfacial Ti atoms.

First of all, one immediately observes a similarity among the three reduced phases but with a greater similarity between the *z*′- and *w*-phases, consistent with the structural models of Figures 3 and 4, where they both have almost the same stoichiometry. On the other hand, the experimentally observed shift of the broadband, mainly O 2p in character, of the *z*-phase to lower BE with respect to those of the *z*′- and *w*-phases is compatible with the theoretical trend. This is the result of a corresponding shift in the O PDOS, which dominate the WDOS over nearly the entire range, pointing to the fact that the oxygen atoms are less negatively charged in the *z*-phase with respect to the *z*′- and *w*-phases. It can be noted that this effect is much less pronounced in the Ti PDOS, which remains more or less identical in the three NLs (in agreement with the Ti 2p XPS data). This phenomenon can be rationalized in terms of a depolarization mechanism of these polar NLs, implying a larger charge transfer from the Pt support to the oxide layer, and thus a shift especially of the O orbitals to lower BE for the phases whose interfacial Ti atoms are formally more oxidized.

4. Conclusions

The structure and the electronic properties of reduced TiO_x polar NLs on Pt(111) have been investigated via DF simulations and comparison with available experimental data. From an analysis of the results, three main conclusions can be drawn.

First of all, we find an inherent similarity among these reduced phases. This is shown by several indicators, such as the fact that we are able to set up atomistic models for these phases on the basis of a common set of building principles, the similar appearance of the VB-UPS and XPS spectra and of the corresponding theoretical PDOS and WDOS, and a linear correlation between the formation energies of these NLs and their formal stoichiometry. In particular, it is confirmed that the STM images at positive bias in the compact regions of these phases can be rationalized by associating bright spots to Ti atoms, whose relative brightness is roughly proportional to the number of coordinating oxygens (more subtle variations are instead found at borderline regions).

Second, it is found that metallization is the actual depolarization mechanism for these NLs. As shown by an analysis of the XPS and VB-UPS spectra and the theoretical DOS, there is a charge transfer from the Pt(111) slab to the oxide NL, so that the Ti atoms at the interface are strongly affected by the underlying support and their actual electronic state is essentially constant (it does not correlate with their formal charge), whereas the trend in the electronic state of the oxygen atoms is counterintuitive: they are the less negative the lower the TiO_x stoichiometry.

Third, subtle effects are at the origin of the large variety of possible structures and kinetic effects during their synthesis can play a role in driving toward a specific phase. This is particularly evident in the case of *w*-NL, which has a similar stoichiometry to that of *z*′-NL but a lower stability, and whose formation must thus be connected with extrinsic causes such as the alloying of incoming Ti atoms with the underlying Pt support.

Acknowledgment. This work has been funded by the European Community through two STRP projects: GSOMEN and NanoChemSens within the SIXTH FRAMEWORK PROGRAMME, by the Italian Ministry of Instruction, University and Research (MIUR) through the fund PRIN-2005, project title: "Novel electronic and chemical properties of metal oxides by doping and nanostructuring", and by the University of Padova, through the grant CPDA071781. Calculations have been performed at Cineca (Bologna, Italy) through an agreement with Italian CNR-INFM.

References and Notes

(1) Hagfeldt, A.; Grätzel, M. *Chem. Rev.* **1995**, *95*, 49.
(2) Carp, O.; Huisman, C. L.; Reller, A. *Prog. Solid State Chem.* **2004**, *32*, 33.
(3) Riu, J.; Maroto, A.; Rius, F. X. *Talanta* **2006**, *69*, 288.
(4) (a) Paulose, M.; Varghese, O., K.; Mor, G. K.; Grimes, C. A.; Ong, K. G. *Nanotechnology* **2006**, *17*, 398. (b) Chen, X.; Mao, S. S. *Chem. Rev.* **2007**, *107*, 2891.
(5) Schoiswohl, J.; Surnev, S; Netzer, F. P.; Kresse, G. *J. Phys.: Condens. Matter* **2006**, *18*, R1.
(6) Schoiswohl, J.; Sock, M.; Chen, Q.; Thornton, G.; Kresse, G.; Ramsey, M. G.; Surnev, S; Netzer, F. P. *Top. Catal.* **2007**, *46*, 137.
(7) Netzer, F. P. *Surf. Rev. Lett.* **2002**, *4*, 1553.
(8) Diebold, U. *Surf. Sci. Rep.* **2003**, *48*, 53.
(9) Papageorgiou, A. C.; Pang, C. L.; Chen, Q.; Thornton, G. *ACS Nano* **2007**, *1*, 409.
(10) Sedona, F.; Rizzi, G. A.; Agnoli, S.; Llabres i Xamena, F. X.; Papageorgiou, A.; Osterman, D.; Sambi, M.; Finetti, P.; Schierbaum, K.; Granozzi, G. *J. Phys. Chem. B* **2005**, *109*, 24411.
(11) Sedona, F.; Agnoli, S.; Granozzi, G. *J. Phys. Chem. B* **2006**, *110*, 15359.
(12) Barcaro, G.; Sedona, F.; Fortunelli, A.; Granozzi, G. *J. Phys. Chem. C* **2007**, *111*, 6095.
(13) Sedona, F.; Granozzi, G; Barcaro, G.; Fortunelli, A. *Phys. Rev. B* **2008**, *77*, 115417.
(14) Tauster, S. J.; Fung, S. C.; Garten, J. *J. Am. Chem. Soc.* **1978**, *100*, 170.
(15) Finetti, P.; Sedona, F.; Rizzi, G. A.; Mick, U.; Sutara, F.; Svec, M.; Matolin, V.; Schierbaum, K.; Granozzi, G. *J. Phys. Chem. C* **2007**, *111*, 869.
(16) Schmid, M.; Kresse, G.; Buchsbaum, A.; Napetschnig, E.; Gritschneder, S.; Reichling, M.; Varga, P. *Phys. Rev. Lett.* **2007**, *99*, 196104.
(17) Berdunov, N.; Mariotto, G.; Balakrishnan, K.; Murphy, S.; Shvets, I. V. *Surf. Sci.* **2006**, *600*, L287.
(18) Hamm, G.; Becker, C.; Henry, C. R. *Nanotechnology* **2006**, *17*, 1943.
(19) Sedona, F.; Agnoli, S.; Fanetti, M.; Kholmanov, I.; Cavaliere, E.; Gavioli, L.; Granozzi, G. *J. Phys. Chem. C* **2007**, *111*, 8024.
(20) Barcaro, G.; Fortunelli, A.; Granozzi, G. *Phys. Chem. Chem. Phys.* **2008**, *10*, 1876.
(21) Baroni, S.; Dal Corso, A.; de Gironcoli, S.; Giannozzi, P. 2007. http://www.pwscf.org.
(22) Vanderbilt, D. *Phys. Rev. B* **1990**, *41*, 7092.
(23) Perdew, J. P.; Chevary, J. A.; Vosko, S. H.; Jackson, K. A.; Pederson, M. R.; Singh, D. J.; Fiolhais, C. *Phys. Rev. B* **1992**, *46*, 6671.
(24) Bengtsson, L. *Phys. Rev. B* **1999**, *59*, 12301.
(25) Tersoff, J; Hamann, D. R. *Phys. Rev. Lett.* **1998**, *50*, 1993.
(26) Wang, Y.; Doren, D. J. *Solid State Commun.* **2005**, *136*, 186.
(27) Finazzi, E.; Di Valentin, C.; Pacchioni, G.; Selloni, A. *J. Chem. Phys.* **2008**, *129*, 154113.
(28) http://www.elettra.trieste.it.

(29) Mekata, M. *Phys. Today* **2003**, *56*, 12.
(30) Sedona, F.; Sambi, M.; Artiglia, L.; Rizzi, G. A.; Vittadini, A.; Fortunelli, A.; Granozzi, G. *J. Phys. Chem. C* **2008**, *112*, 3187.
(31) Hsieh, S.; Matsumoto, T.; Batzill, M.; Koel, B. E. *Phys. Rev. B* **2003**, *68*, 205417.
(32) Bennett, R. A.; Pang, C. L.; Perkins, N.; Smith, R. D.; Morrall, P.; Kvon, R. I.; Bowker, M. *J. Phys. Chem. B* **2002**, *106*, 4688.
(33) Reuter, K.; Scheffler, M. *Phys. Rev. B* **2002**, *65*, 035406.
(34) Hsieh, S.; Liu, G. F.; Koel, B. E. *J. Vac. Sci. Technol., A* **2008**, *26*, 1336.
(35) Yeh, J. J.; Lindau, I. *Atomic Data and Nuclear Data Tables* **1985**, *32*, 1.

JP811020S